

# Transistors based on Novel 2-D Monolayer Semiconductors $\text{Bi}_2\text{O}_2\text{Se}$ , $\text{InSe}$ , and $\text{MoSi}_2\text{N}_4$ for Enhanced Logic Density Scaling

Keshari Nandan, *Member, IEEE*, Ateeb Naseer, *Graduate Student Member, IEEE*, Amit Agarwal, Somnath Bhowmick, Yogesh S. Chauhan, *Fellow, IEEE*

**Abstract**—Making ultra-short gate-length transistors significantly contributes to scaling the contacted gate pitch. This, in turn, plays a vital role in achieving smaller standard logic cells for enhanced logic density scaling. As we push the boundaries of miniaturization, it is intriguing to consider that the ultimate limit of contacted gate pitch could be reached with remarkable 1 nm gate-length transistors. Here, we identify  $\text{InSe}$ ,  $\text{Bi}_2\text{O}_2\text{Se}$ , and  $\text{MoSi}_2\text{N}_4$  as potential two-dimensional semiconductors for 1 nm transistors with low contact resistance and outstanding interface properties. We employ a fully self-consistent ballistic quantum transport model starting from first-principle calculations. Our simulations show that the interplay between electrostatics and quantum tunneling influences the performance of these devices over the device design space.  $\text{MoSi}_2\text{N}_4$  channels have the best immunity to quantum tunneling, and  $\text{Bi}_2\text{O}_2\text{Se}$  channel devices have the best electrostatics. We show that for a channel length of 12 nm, all the devices can deliver  $I_{\text{ON}}/I_{\text{OFF}} > 10^3$ , suitable for electronic applications, and  $\text{Bi}_2\text{O}_2\text{Se}$  is the best-performing channel material.

**Index Terms**—Field-effect transistors, 1 nm gate length,  $\text{Bi}_2\text{O}_2\text{Se}$ ,  $\text{MoSi}_2\text{N}_4$ ,  $\text{InSe}$

## I. INTRODUCTION

FETs based on 2-D channel materials are more immune to short-channel effects (SCEs) and offer better device scaling [1], [2]. In ultra-thin-body devices, they show superior gate control and better mobility than bulk semiconductors such as Si, Ge, and III-V. In recent years, experimental 2-D FETs have shown ideal performance. In addition, one can integrate a 2-D channel with a 1-D metallic nanowire, nanotube, or 2-D graphene as the gate. This integration facilitates 1 nm and sub-1 nm gate lengths in 2-D FETs [3]–[8]. Considering the interface quality of the gate stack, metal contact with 2-D semiconductors, and quality of the grown channel, we study a

few potential contenders for the channel material in ultra-short 2-D FETs. They are monolayers of  $\text{MoSi}_2\text{N}_4$ ,  $\text{Bi}_2\text{O}_2\text{Se}$ , and  $\text{InSe}$ .

$\text{MoSi}_2\text{N}_4$  was synthesized in 2020, showing excellent physical, mechanical, thermal, electronic, and metal contact properties [9]–[12]. It outperforms most other 2-D semiconductors and shows excellent ohmic contact with CMOS-compatible metals [10].  $\text{Bi}_2\text{O}_2\text{Se}$  is a ternary semiconducting compound with outstanding stability and a moderate bandgap [13], [14]. High- $k$  native crystalline oxide dielectric,  $\text{Bi}_2\text{SeO}_5$ , can be formed by layer-by-layer oxidation of  $\text{Bi}_2\text{O}_2\text{Se}$ . At wafer-scale,  $\text{Bi}_2\text{O}_2\text{Se}$  FETs can be fabricated using this native oxide as gate oxide with EOT below sub-0.5 nm [15]. The performance of wafer-scale  $\text{Bi}_2\text{O}_2\text{Se}$  based FinFETs with  $\text{Bi}_2\text{SeO}_5$  as gate insulators is competitive to Si and Ge-based FinFETs. These  $\text{Bi}_2\text{O}_2\text{Se}$  FinFETs show low contact resistance,  $R_C \sim 470 \Omega \mu\text{m}$  [16].  $\text{InSe}$  FETs have shown ideal performance close to the ballistic limit down to 10 nm gate length with a power supply voltage of 0.5 V and low contact resistance,  $R_C \sim 65 \Omega \mu\text{m}$  [17]. Wafer-scale  $\text{InSe}$  meets the standard for electronic-grade semiconductor material [18]. These are ideal atomic thin channel materials for next-generation logic design and monolithic three-dimensional (M3D) integration with state-of-the-art Si devices.

Here, we explore the potential of  $\sim 1$  nm gate-length transistors using novel 2-D semiconducting monolayers, highlighting their excellent performance characteristics and role in advancing electronic device miniaturization. Our research highlights the role of geometrical and material parameters—such as the nanowire gate, spacer, gate dielectric, and channel length—within integrated 2-D channel FETs featuring metallic nanowires. Considering the favorable figures for 2-D semiconductors for the transistor’s channel, we choose monolayers of  $\text{MoSi}_2\text{N}_4$ ,  $\text{Bi}_2\text{O}_2\text{Se}$ , and  $\text{InSe}$  as channels in our research. The possibility of integrating a 2-D channel with a 1-D metallic nanowire as a gate alleviates the lithography limitation on gate patterning [3]–[6]. This configuration allows one to realize the scaling potential of 2-D FETs, thanks to their natural atomic-scale dimensions. The key findings of our research are the following:

- The fringing field from the nanowire gate enhances gate efficiency, which in turn improves gate control over the channel for a given gate oxide. When the spacer material

K. Nandan was with the Department of Electrical Engineering, IIT Kanpur, Kanpur 208016, India. He is now with the Department of Electrical and Computer Engineering, University of Minnesota, Minneapolis MN 55455, USA (e-mail: knandan@umn.edu).

A. Naseer and Y. S. Chauhan are with the Department of Electrical Engineering, IIT Kanpur, Kanpur 208016, India (e-mail: chauhan@iitk.ac.in).

A. Agarwal is with the Department of Physics, IIT Kanpur, Kanpur 208016, India.

S. Bhowmick is with the Department of Materials Science and Engineering, IIT Kanpur, Kanpur 208016, India.

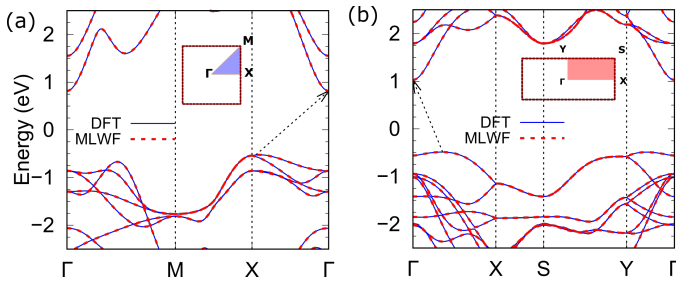


**Fig. 1.** Comparison of band structure calculated from DFT and tight-binding Hamiltonian (in MLWFs basis) along high symmetry paths in the Brillouin zone for (a)  $\text{Bi}_2\text{O}_2\text{Se}$  and (b)  $\text{InSe}$ . The band structure from MLWFs Hamiltonian shows good agreement with DFT in the vicinity of conduction band minima and valance band maxima. Fermi energy level is shifted to zero energy.

is changed from air to  $\text{SiO}_2$ , gate efficiency improves by 75%, leading to better switching characteristics for the devices.

- Slight performance improvements are observed when using  $\text{CaF}_2$  as both the spacer and gate oxide, compared to  $\text{SiO}_2$  (as both the spacer and gate oxide) with the same EOT. This is mainly due to the increased physical thickness of the  $\text{CaF}_2$  gate oxide, which reduces the benefits of having a higher- $k$  spacer (see Fig. 3 and Table I). Although a higher- $k$  spacer (with greater permittivity than  $\text{CaF}_2$ ) can provide some advantages, it also introduces increased cross-talk, which is undesirable. Moreover, reducing the gate oxide thickness proves beneficial for a given spacer.
- As the gate oxide thickness increases, the gate's control over the channel weakens due to reduced gate oxide capacitance and decreased fringing capacitance from the gate. This results in a logarithmic relationship between the subthreshold slope and gate oxide thickness, contrasting with conventional FETs [19], [20].
- Increasing the dimensions of the gate uniformly improves switching metrics for a given channel length, and the reverse is also true. However, altering the gate shape from square to triangular degrades the device's performance due to increased direct source-to-drain tunneling.  $\text{MoSi}_2\text{N}_4$  demonstrates greater resistance to this type of tunneling. For instance, the subthreshold swing and on-state current deteriorate by approximately 14.5% and 53%, respectively, when changing the nanowire gate structure from square to triangular. In contrast,  $\text{Bi}_2\text{O}_2\text{Se}$  and  $\text{InSe}$  devices experience significant leakage due to severe direct tunneling, attributed to their low carrier effective mass.
- Ultra-scaled FETs with these promising 2-D semiconducting channels achieve  $I_{\text{ON}}/I_{\text{OFF}} > 10^3$  with  $SS < 130$  mV/decade.  $\text{Bi}_2\text{O}_2\text{Se}$  stands out, closely followed by  $\text{InSe}$  and  $\text{MoSi}_2\text{N}_4$ .

## II. METHODOLOGY

To model the full-band transport in the devices, an accurate model Hamiltonian for the channel is required [21]. For this, the electronic properties of channel material are characterized

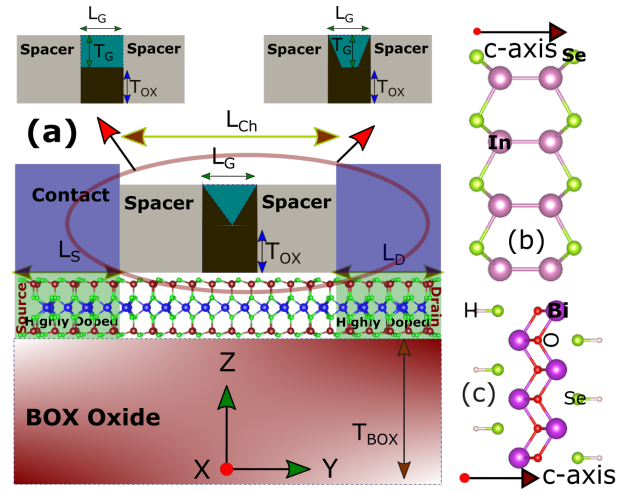


**Fig. 2.** (a) Schematic of top-gated monolayer 2-D FETs with different gate structures like square, rectangle, isosceles, and triangle. The channel comprises of monolayer  $\text{MoSi}_2\text{N}_4$ .  $\text{SiO}_2$  is used as BOX oxide with a thickness of  $T_{\text{BOX}}$ . The gate is of metal and separated from the channel by  $T_{\text{OX}}$ . Side view of the atomic structure of (b)  $\text{InSe}$  and (c)  $\text{Bi}_2\text{O}_2\text{Se}$ .

from first- principles by combining the power of density-functional theory (DFT) [22] and maximally localized Wannier functions (MLWFs) [23]. The optimized structural parameters and bandgap values agree well with the literature. All these are indirect bandgap semiconductors, whose bandgap value lies in the range 1.3-1.9 eV:  $\text{InSe} \sim 1.52$  eV,  $\text{Bi}_2\text{O}_2\text{Se} \sim 1.34$  eV, and  $\text{MoSi}_2\text{N}_4 \sim 1.84$  eV. Model Hamiltonian validation against DFT results involves calculating eigenenergies along high symmetry points. The band structure from our model demonstrates good agreement with DFT, particularly around the bandgap (for example, see Fig. 1 for  $\text{Bi}_2\text{O}_2\text{Se}$  and  $\text{InSe}$ ).

The charge density in the channel is obtained by estimating the Green's functions in the non-equilibrium Green's function (NEGF) formalism [24]. The channel charge is included in Poisson's equation to determine the converged physical observables of the system [25]. Green's function is obtained by uniformly sampling the transverse wavevectors with 30 sampling points. The source-to-drain current is calculated by Landauer-Büttiker approach [26]. The device structure is shown in Fig. 2 (a), which is analogous to experimental structures in [4], [6]. The side view of the atomic structure of  $\text{MoSi}_2\text{N}_4$ ,  $\text{InSe}$ , and  $\text{Bi}_2\text{O}_2\text{Se}$  is also shown in Fig. 2. Fig. 3 shows the relative comparison of gate stacks between two different gate DE, both having the same EOT of 1 nm. Considering the ultra-low contact resistance and stability of 2-D devices contacted with semimetal, we mimic the degenerate state for the semiconductor in contact with semimetal by chemically doping the source and drain regions in our simulations [17], [27]–[29]. These results should be regarded as the upper limit for device performance, as non-ideal effects are not considered here. All device simulations are carried out at room temperature.

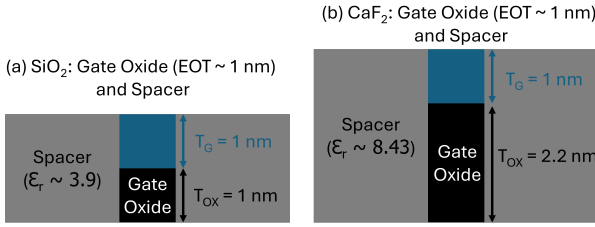


Fig. 3. The relative comparison between (a) the SiO<sub>2</sub> spacer with a SiO<sub>2</sub> gate dielectric and (b) the CaF<sub>2</sub> spacer with a CaF<sub>2</sub> gate dielectric, both having the same EOT of 1 nm, shows that the increased  $T_{OX}$  in (b) results in only a slight improvement in gate control compared to (a).

### III. RESULTS AND DISCUSSION

To capture the switching behavior in these ultra-scaled logic devices, we begin with the monolayer MoSi<sub>2</sub>N<sub>4</sub> channel. The gate dimensions are 1 nm × 1 nm, and equivalent oxide thickness (EOT) is 1 nm. The transfer characteristics on the semilogarithmic scale are shown in Fig. 4 (a) for the air spacer with SiO<sub>2</sub> gate dielectric, the SiO<sub>2</sub> spacer with SiO<sub>2</sub> gate dielectric, and the calcium fluoride (CaF<sub>2</sub>) spacer with CaF<sub>2</sub> gate dielectric with  $L_{Ch} = 12$  nm. Ensuring a high-quality integration of 2-D channels with high- $k$  oxides is paramount. Epitaxial CaF<sub>2</sub> can establish a quasi-van der Waals contact with 2-D semiconductors [30], [31], resulting in excellent interface quality. Also, it can serve as an ultrathin gate insulator with a high dielectric constant ( $\epsilon = 8.43$ ) for 2-D devices with an equivalent oxide thickness (EOT) down to 1 nm and minimal leakage current ( $I_{ON}/I_{OFF} > 10^7$ ) [32]. For EOT values of 0.5 nm and 1 nm, 2-D devices with CaF<sub>2</sub> gate stack show lower leakage than other high- $k$  oxides, like HfO<sub>2</sub> and La<sub>2</sub>O<sub>3</sub> [32]. Conversely, defects can adversely impact metal-oxide-semiconductor field-effect transistors (MOSFETs) by causing issues such as charge trapping and de-trapping, bias temperature instabilities (BTI) (driven by charge de-trapping), and mobility degradation (due to coulomb scattering from trapped charges in the oxide) [30].

#### A. Role of Gate Oxide and Spacer

We observe that effective channel length ( $L_{eff}$ ) increases (see Fig. 4 (b-d)), and switching characteristics improve with an increase in the spacer's permittivity. This improvement is attributed to increased parasitic capacitance arising from the fringing field from gate [33],  $C_{par} \sim \epsilon_{spacer} \times \ln(1 + T_G/T_{ox})$ , where  $\epsilon_{spacer}$  is the permittivity of spacer. The device with air spacer shows poor switching characteristics with gate efficiency  $< 0.3$  and subthreshold slope,  $SS \sim 236$  mV/decade with the ON to the OFF current ratio,  $I_{ON}/I_{OFF} > 10^2$ . Gate efficiency is defined as  $-\Delta\phi_b/\Delta V_{GS}$  in the subthreshold regime, where  $\phi_b$  is the source-to-channel barrier height. The simulations are carried out at  $V_{DS} = 0.5$  V, where  $V_{DS}$  denotes the drain to source voltages. The  $V_{OFF}$  voltage is the gate voltage,  $V_{GS}$ , that produces a drain current  $I_{DS}$  equal to a specified  $I_{OFF} \sim 10^{-1}$   $\mu A/\mu m$ . The  $I_{ON}$  of a FET is measured at the ON-state voltage  $V_{ON} = V_{OFF} + V_{DD}$ , where  $V_{DD} = 0.5$  V is the power supply voltage. Replacing

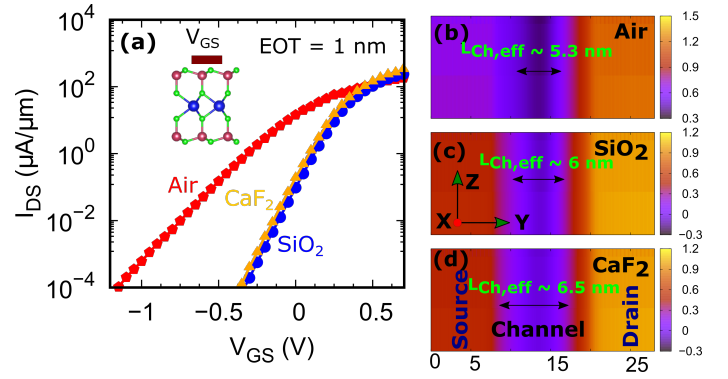


Fig. 4. (a) Transfer characteristics of ultra-short 2-D FETs comprised of MoSi<sub>2</sub>N<sub>4</sub> for air spacer with SiO<sub>2</sub> gate dielectric, SiO<sub>2</sub> spacer with SiO<sub>2</sub> gate dielectric, and CaF<sub>2</sub> spacer with CaF<sub>2</sub> gate dielectric.  $L_{Ch} \sim 12$  nm and  $T_G \times L_G = 1$  nm × 1 nm. The surface plot of the potential profile in the source, channel, and drain for (b) air spacer, (c) SiO<sub>2</sub> spacer, and (d) CaF<sub>2</sub> spacer at  $V_{DS} = 0.5$  V and  $V_{GS} = -0.5$  V. An increase in the dielectric constant of the spacer results in better gate efficiency and, therefore, a larger effective channel length,  $L_{Ch,eff}$ . The device with an air spacer has the worst gate efficiency.

the spacer with higher permittivity improves the switching characteristics. For example, SiO<sub>2</sub> spacer improves the gating efficiency by 75%, therefore better switching characteristics ( $SS \sim 129$  mV/decade) and  $I_{ON}/I_{OFF} (> 10^3)$ . However, small performance improvements are observed in the case of CaF<sub>2</sub> as both spacer and gate oxide, compared to SiO<sub>2</sub> (as both spacer and gate oxide). This is primarily due to its increased gate oxide physical thickness, which diminishes the impact of having higher- $k$  spacer (see Fig. 3 and Table I). Building on this analysis, we further demonstrate the impact of spacers with CaF<sub>2</sub> gate oxide. The results indicate that while a higher- $k$  spacer (with greater permittivity than CaF<sub>2</sub>) can offer advantages, it comes at the cost of increased cross-talk, which is undesirable. Additionally, reducing the gate oxide thickness proves advantageous within the given spacer configuration.

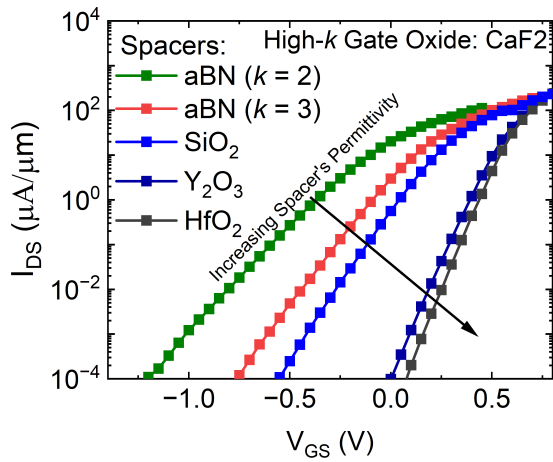
Further, we assessed the performance of ultra-short devices with various spacers, ranging from low- $k$  to high- $k$  materials, using CaF<sub>2</sub> as a high- $k$  gate dielectric (see Fig. 5), which is ideally suited for 2-D channel materials. Performance improvements are noted when  $k > 8$ , but this range is less favorable due to heightened electronic cross-talk. To analyze the impact of physical gate oxide thickness, we consider low- $k$  spacer with permittivity of 3 and CaF<sub>2</sub> as high- $k$  gate oxide. We perform the analysis with different gate oxide

TABLE I

SUBTHRESHOLD SLOPE ( $SS$ ), ON-STATE CURRENT ( $I_{ON}$ ), AND ON CURRENT TO THE OFF CURRENT RATIO ( $I_{ON}/I_{OFF}$ ) FOR DIFFERENT COMBINATIONS OF THE GATE OXIDES AND SPACERS.

Gate Oxide	Spacer	$SS$ (mV/decade)	$I_{ON}$ ( $\mu A/\mu m$ )	$I_{ON}/I_{OFF}$
SiO <sub>2</sub>	Air	236	18.45	$1.84 \times 10^2$
SiO <sub>2</sub>	SiO <sub>2</sub>	128.98	106.67	$1.07 \times 10^3$
CaF <sub>2</sub>	CaF <sub>2</sub>	124.90	117.62	$1.18 \times 10^3$





**Fig. 5.** Transfer characteristics of ultra-short 2-D FETs, showing the role of spacer. The channel is comprised of  $\text{MoSi}_2\text{N}_4$ , and  $\text{CaF}_2$  is used as the high- $k$  gate dielectric.  $L_{\text{Ch}} \sim 12$  nm and  $T_{\text{G}} \times L_{\text{G}} = 1$  nm  $\times$  1 nm. Small performance gains are observed when  $k > 8$ , though this range is less favorable due to increased electronic cross-talk.

thicknesses ( $T_{\text{OX}}$ ), ranging from 3.3 nm (EOT  $\sim 1.5$  nm) down to 1.1 nm (EOT  $\sim 0.5$  nm). As the oxide thickness ( $T_{\text{OX}}$ ) increases for a given gate oxide, gate dimensions, and spacer configuration, the gate's control over the channel weakens. This occurs due to a combination of effects from the gate oxide capacitance and fringing capacitance caused by the spacer. The gate oxide capacitance decreases when the gate oxide thickness increases, reducing the gate's control. Additionally, the fringing capacitance from the spacer plays a role in gate control in short-channel devices. An increase in  $T_{\text{OX}}$  decreases parasitic capacitance, further weakening the gate's control, and conversely, reducing  $T_{\text{OX}}$  increases parasitic capacitance, enhancing the gate's control over the channel. To show the impact of  $T_{\text{OX}}$  quantitatively, we plot the transfer characteristics with different  $T_{\text{OX}}$  ranging from 3.3 nm down to 1.1 nm (see Fig. 6). This  $T_{\text{OX}}$  variation is equivalent to EOT's variation from 1.5 nm down to 0.5 nm. The channel is comprised of  $\text{MoSi}_2\text{N}_4$ ,  $\text{CaF}_2$  is used as gate dielectric, and aBN is used as low- $k$  spacer. The  $SS$  is plotted with  $T_{\text{G}}/T_{\text{OX}}$  in inset of Fig. 6. Unlike conventional FETs [19], [20], the  $SS$  versus  $T_{\text{OX}}$  trend is logarithmic with  $T_{\text{OX}}$  due to the role of fringing in determining the gate control. Further study considers  $\text{SiO}_2$  to be both a spacer and gate oxide. The gate oxides and spacers are considered perfect insulators.

### B. Role of Channel Materials

For 2-D semiconductors, the centroid capacitance is often assumed to be infinite [34], therefore  $C_{\text{S}} \sim C_{\text{Q}}$ , where  $C_{\text{S}}$  is the capacitance of the channel material and  $C_{\text{Q}}$  is the quantum capacitance of the channel material. Therefore,  $SS$  is proportional to  $(1 + C_{\text{Q}}/C_{\text{OX}})$  in the negligible tunneling regime [35]. Thus, a lower quantum capacitance channel would be beneficial in reducing the thermionic  $SS$  [36]. This is evident from the subthreshold slope of the thermionic current,  $SS_{\text{thermal}}$ . It is the best for the  $\text{Bi}_2\text{O}_2\text{Se}$  channel ( $\sim 98$  mV/decade) and slightly degrades for InSe ( $\sim 100$

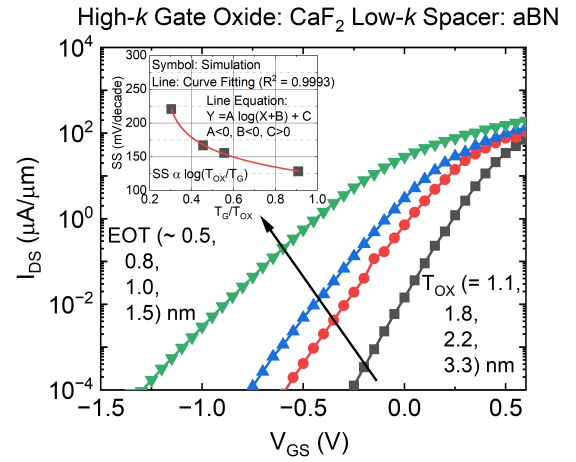


**Fig. 6.** Transfer characteristics of ultra-short 2-D FETs, showing the role of gate oxide thickness scaling. The channel is comprised of  $\text{MoSi}_2\text{N}_4$ ,  $\text{CaF}_2$  is high- $k$  gate dielectric, and amorphous boron nitride (aBN) is low- $k$  spacer.  $L_{\text{Ch}} \sim 12$  nm and  $T_{\text{G}} \times L_{\text{G}} = 1$  nm  $\times$  1 nm. In the inset,  $SS$  is plotted with  $T_{\text{G}}/T_{\text{OX}}$ . Unlike conventional FETs, this trend is logarithmic with  $T_{\text{OX}}$ .

mV/decade) compared to  $\text{Bi}_2\text{O}_2\text{Se}$ . As the quantum capacitance values are approximately similar for InSe ( $m_e \sim 0.205m_0$  and  $g_v = 1$ ) and  $\text{Bi}_2\text{O}_2\text{Se}$  ( $m_e \sim 0.197m_0$  and  $g_v = 1$ ), both being less than one-fourth of  $\text{MoSi}_2\text{N}_4$  ( $m_e \sim 0.48m_0$  and  $g_v = 2$ ). For  $\text{MoSi}_2\text{N}_4$ , the subthreshold slope is the worst, close to 125 mV/decade. The thermionic current component is plotted in Fig. 7 (a), providing a zoomed view of the subthreshold regime. However, at a channel length of  $L_{\text{Ch}} = 12$  nm, the switching behavior is influenced by both direct tunneling leakage and electrostatics. The contribution of direct tunneling from source-to-drain in the off-state current,  $I_{\text{OFF}}$ , is significant for InSe ( $\sim 54\%$ ) and  $\text{Bi}_2\text{O}_2\text{Se}$  ( $\sim 59\%$ ) but lower for  $\text{MoSi}_2\text{N}_4$  ( $\sim 12\%$ ). The strength of InSe and  $\text{Bi}_2\text{O}_2\text{Se}$  are better electrostatic control in the devices comprised of them. Even in the presence of large direct tunneling, InSe and  $\text{Bi}_2\text{O}_2\text{Se}$  demonstrate better control over the switching behavior compared to  $\text{MoSi}_2\text{N}_4$  for  $L_{\text{Ch}} = 12$  nm (see Fig. 7).

Devices comprised of these promising 2-D semiconducting channels can deliver  $I_{\text{ON}}/I_{\text{OFF}} > 10^3$  with  $SS < 130$  mV/decade.  $\text{Bi}_2\text{O}_2\text{Se}$  is the best-performing channel material ( $SS \sim 109$  mV/decade and  $I_{\text{ON}} \sim 186$   $\mu\text{A}/\mu\text{m}$ ) and the performance of the InSe ( $SS \sim 112$  mV/decade and  $I_{\text{ON}} \sim 153$   $\mu\text{A}/\mu\text{m}$ ) is close to  $\text{Bi}_2\text{O}_2\text{Se}$ , followed by  $\text{MoSi}_2\text{N}_4$ . The  $I_{\text{ON}}/I_{\text{OFF}}$  of all these three channel materials are one order higher than 1 nm  $\text{MoS}_2$  FET with a circular metallic gate of diameter 1 nm with 10 nm channel length ( $SS \sim 160$  mV/decade and  $I_{\text{ON}}/I_{\text{OFF}} \sim 400$ ) [37]. Increasing the  $L_{\text{Ch}}$  degrades the control of the gate over the channel and, on the contrary, reduces the impact of direct tunneling (because of increased tunneling barrier height and width) and vice versa (see Fig. 9 (a)). This device configuration comprises these novel 2-D semiconductors and can deliver better switching performance than other ultra-short device configurations like FETs with core-shell nanowire gates [3], [7].

In the quest of performance improvement, applying 1%

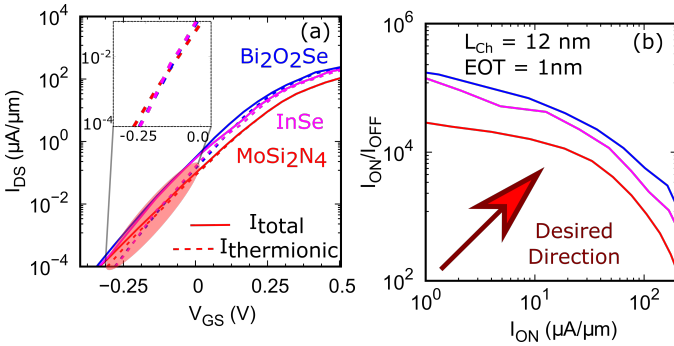


Fig. 7. (a) Benchmarking of transfer characteristics and (b)  $I_{ON}/I_{OFF}$  vs.  $I_{ON}$  for three promising 2-D semiconductors as a channel in ultra-short FET architecture.  $SiO_2$  is used as gate oxide with  $EOT = 1$  nm, spacer, and BOX oxide with  $T_{BOX} = 10$  nm. The channel length is 12 nm,  $T_G \times L_G = 1$  nm  $\times$  1 nm, and  $V_{DS} = 0.50$  V.  $Bi_2O_2Se$  device shows the best switching characteristic and  $I_{ON}$  for a given  $I_{ON}/I_{OFF}$ .

tensile strain along the channel direction, which is reasonable in experiments with flexible substrates [38], [39], leads to minor change in performance of the FETs compared to pristine channel FETs. As, it can lower the  $C_Q$  by 3.8%, -0.25%, and -0.005% in  $MoSi_2N_4$ ,  $Bi_2O_2Se$ , and  $InSe$ , respectively, than a pristine channel. The decrease in bandgap is less than 6% compared to pristine monolayers, which is suitable for mitigating intra-band tunneling leakage. Another possible solution could be utilizing the non-linear dielectric response of dielectric-ferroelectric (DE-FE) [40] stacked or FE-antiferroelectric (FE-AFE) [41] stacked materials in the gate-stack. This is a promising approach to enhance the performance of devices by amplifying the surface potential's response to changes in gate voltage.

### C. Role of Gate's dimensions and Performance Metrics

The role of gate geometry and dimensions is also studied for better assessment of device performance over design space. We find that a uniform increment in  $T_G$  and  $L_G$  improves the switching metrics for a given channel length and vice versa. For example, a change in gate dimensions from  $0.5 \times 0.5$  to  $2 \times 2$ , improves the gate efficiency by  $\sim 45\%$ ,  $SS$  by  $\sim 30\%$ , and  $I_{ON}$  by  $\sim 215\%$  in  $MoSi_2N_4$  devices. Increasing gate height from 0.1 nm to 2 nm with  $L_G$  of 1 nm enhances the gate efficiency by  $\sim 34\%$ ,  $SS$  by  $\sim 31\%$ , and  $I_{ON}$  by  $\sim 189\%$ . The gate geometry variations, from square to triangular, are characterized by an angle  $\theta$  (in degrees). For  $MoSi_2N_4$ , the  $SS$  and  $I_{ON}$  are deteriorated by  $\sim 14.5\%$  and  $53\%$ , respectively, while varying the gate structure from square ( $\theta = 90$ ) to triangular ( $\theta = 63.44$ ). For  $\theta > 72$  (78), the degradation in  $I_{ON}$  is less than 32% (23%), see Fig. 8. For  $Bi_2O_2Se$  and  $InSe$  devices, severe direct tunneling results in severe leakage for  $\theta < 73.30$  due to low carrier effective mass.

Finally, critical circuit-level performance metrics are estimated for a chain of inverters with a logic depth of 20, as shown in Fig. 9. We have estimated the delay and energy per operation. These metrics have been normalized by the node capacitance and the total capacitance of the logic design. This

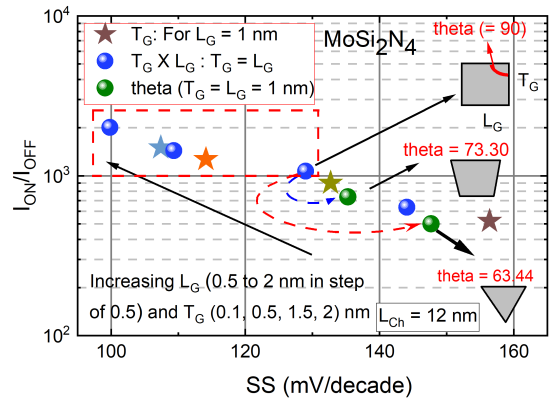


Fig. 8. The role of gate dimensions in the performance of ultra-short channel devices.

normalization approach is reasonable in sub-10 nm technology, as interconnect capacitance becomes the dominant component of total capacitance [42], [43]. For these promising channel materials, the normalized delay ( $\tau$ ) and energy-delay product (EDP) for a chain of 20 inverters are impressively low, measuring less than 95 and 1.5, respectively. To put this into perspective, these circuit-level metrics outperform 1 nm  $MoSi_2$  FET with a circular metallic gate of diameter 1 nm with 10 nm channel length (the  $\tau$  is around 250, and the EDP is approximately 5 [37]).

## IV. CONCLUSION

In the pursuit of identifying promising 2-D semiconductors for cutting-edge electronic applications, we have identified  $MoSi_2N_4$ ,  $InSe$ , and  $Bi_2O_2Se$  as highly promising candidates. By considering the feasibility of integrating metallic nanowires with 2-D semiconductors, we have investigated their suitability as channel materials within an innovative device structure. Our goal is to harness their unique properties and capabilities for ultra-scaled FETs with ultra-scaled gate lengths (approximately 1 nm). We have found that the  $Bi_2O_2Se$  FET exhibits the most favorable switching metrics and circuit-level performance.  $InSe$  FETs perform closely to  $Bi_2O_2Se$ , with  $MoSi_2N_4$  following closely behind.

Beyond its applications in logic circuits, this novel device structure has the potential to be extended into a multi-gate configuration model [6]. This extension opens up exciting possibilities for achieving precise and localized control over band structures, which in turn enables the design of more integrated, multifunctional, and highly controllable nanodevices. Moreover, this versatile device topology can also find utility in the development of ultra-low-power spiking neurons, particularly for neuromorphic applications [44]. This represents an exciting direction where the technology can contribute to the advancement of brain-inspired computing.

## V. ACKNOWLEDGMENT

The authors thank the HPC facility, IIT Kanpur, Kanpur, India, and the National Supercomputing Mission (NSM) for providing the computational resources. KN is thankful to Ashok for the insightful discussions.

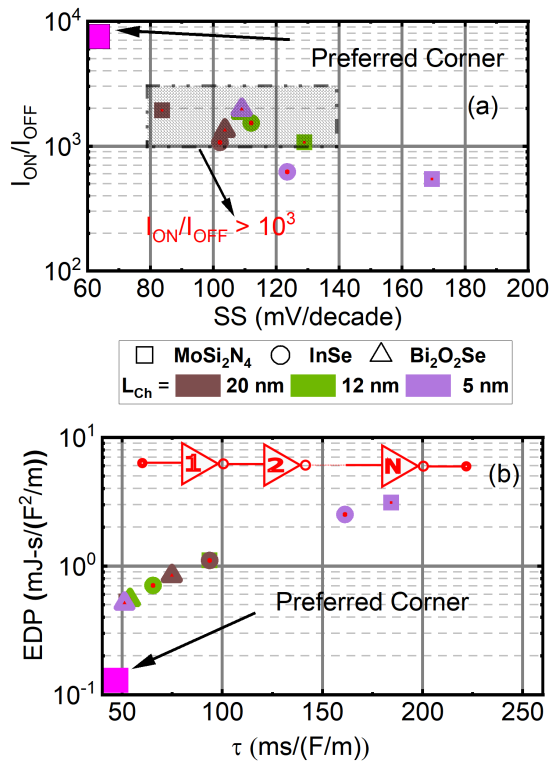


Fig. 9. (a) Benchmarking of switching characteristics (SS versus  $I_{ON}/I_{OFF}$ ) for the devices. (b) Circuit level characteristics ( $\tau$  versus EDP) for a 20-stage inverter comprised of these ultra-short 2-D channel devices.

## REFERENCES

- [1] F. Zhuo, J. Wu, B. Li, M. Li, C. L. Tan, Z. Luo, H. Sun, Y. Xu, and Z. Yu, "Modifying the power and performance of 2-dimensional  $\text{MoS}_2$  field effect transistors," *Research*, vol. 6, p. 0057, 2023, doi: 10.34133/research.0057.
- [2] K. Nandan, A. Agarwal, S. Bhowmick, and Y. S. Chauhan, "Two-dimensional semiconductors based field-effect transistors: review of major milestones and challenges," *Frontiers in Electronics*, vol. 4, 2023, doi: 10.3389/felec.2023.1277927.
- [3] W. Cao, W. Liu, and K. Banerjee, "Prospects of ultra-thin nanowire gated 2d-fets for next-generation cmos technology," in *2016 IEEE International Electron Devices Meeting (IEDM)*, 2016, doi: 10.1109/IEDM.2016.7838419. pp. 14.7.1–14.7.4.
- [4] S. B. Desai, S. R. Madhupathy, A. B. Sachid, J. P. Llinas, Q. Wang, G. H. Ahn, G. Pitner, M. J. Kim, J. Bokor, C. Hu, H.-S. P. Wong, and A. Javey, "MoS<sub>2</sub> transistors with 1-nanometer gate lengths," *Science*, vol. 354, no. 6308, pp. 99–102, 2016, doi: 10.1126/science.aah4698.
- [5] F. Wu, H. Tian, Y. Shen, Z. Hou, J. Ren, G. Gou, Y. Sun, Y. Yang, and T.-L. Ren, "Vertical MoS<sub>2</sub> transistors with sub-1-nm gate lengths," *Nature*, vol. 603, no. 7900, pp. 259–264, Mar 2022, doi: 10.1038/s41586-021-04323-3.
- [6] Y. Xiao, G. Zou, J. Huo, T. Sun, B. Feng, and L. Liu, "Locally thinned, core-shell nanowire-integrated multi-gate MoS<sub>2</sub> transistors for active control of extendable logic," *ACS Applied Materials & Interfaces*, vol. 15, no. 1, pp. 1563–1573, 2023, doi: 10.1021/acsami.2c17788.
- [7] X. Liu, R. Liang, G. Gao, C. Pan, C. Jiang, Q. Xu, J. Luo, X. Zou, Z. Yang, L. Liao, and Z. L. Wang, "MoS<sub>2</sub> negative-capacitance field-effect transistors with subthreshold swing below the physics limit," *Advanced Materials*, vol. 30, no. 28, p. 1800932, 2018, doi: 10.1002/adma.201800932.
- [8] W. Jolie and T. Michely, "1d metals for 2d electronics," *Nature Nanotechnology*, pp. 1–2, 2024.
- [9] Y.-L. Hong, Z. Liu, L. Wang, T. Zhou, W. Ma, C. Xu, S. Feng, L. Chen, M.-L. Chen, D.-M. Sun, X.-Q. Chen, H.-M. Cheng, and W. Ren, "Chemical vapor deposition of layered two-dimensional MoSi<sub>2</sub>N<sub>4</sub> materials," *Science*, vol. 369, no. 6504, pp. 670–674, 2020, doi: 10.1126/science.abb7023.

- [10] Q. Wang, L. Cao, S.-J. Liang, W. Wu, G. Wang, C. H. Lee, W. L. Ong, H. Y. Yang, L. K. Ang, S. A. Yang, and Y. S. Ang, "Efficient ohmic contacts and built-in atomic sublayer protection in  $\text{mosi}_2\text{n}_4$  and  $\text{wsi}_2\text{n}_4$  monolayers," *npj 2D Materials and Applications*, vol. 5, no. 1, p. 71, Aug 2021, doi: 10.1038/s41699-021-00251-y.
- [11] K. Nandan, B. Ghosh, A. Agarwal, S. Bhowmick, and Y. S. Chauhan, "Two-dimensional  $\text{mosi}_2\text{n}_4$ : An excellent 2-d semiconductor for field-effect transistors," *IEEE Transactions on Electron Devices*, pp. 1–8, 2021, doi: 10.1109/TED.2021.3130834.
- [12] K. Nandan, S. Bhowmick, Y. S. Chauhan, and A. Agarwal, "Designing power-efficient transistors using narrow-bandwidth materials from the  $m\text{A}_2\text{Z}_4$  ( $m = \text{Mo, Cr, Zr, Ti, Hf}$ ;  $a = \text{Si, Ge}$ ;  $z = \text{N, P, As}$ ) monolayer series," *Phys. Rev. Appl.*, vol. 19, p. 064058, Jun 2023, doi: 10.1103/PhysRevApplied.19.064058.
- [13] T. Li and H. Peng, "2D  $\text{Bi}_2\text{O}_2\text{Se}$ : An emerging material platform for the next-generation electronic industry," *Accounts of Materials Research*, vol. 2, no. 9, pp. 842–853, 2021, doi: 10.1021/accountsmr.1c00130.
- [14] R. Quhe, J. Liu, J. Wu, J. Yang, Y. Wang, Q. Li, T. Li, Y. Guo, J. Yang, H. Peng *et al.*, "High-performance sub-10 nm monolayer  $\text{Bi}_2\text{O}_2\text{Se}$  transistors," *Nanoscale*, vol. 11, no. 2, pp. 532–540, 2019.
- [15] Y. Zhang *et al.*, "A single-crystalline native dielectric for two-dimensional semiconductors with an equivalent oxide thickness below 0.5 nm," *Nature Electronics*, vol. 5, no. 10, pp. 643–649, Oct 2022, doi: 10.1038/s41928-022-00824-9.
- [16] C. Tan, M. Yu, J. Tang, X. Gao, Y. Yin, Y. Zhang, J. Wang, X. Gao, C. Zhang, X. Zhou, L. Zheng, H. Liu, K. Jiang, F. Ding, and H. Peng, "2D fin field-effect transistors integrated with epitaxial high-k gate oxide," *Nature*, vol. 616, no. 7955, pp. 66–72, Apr 2023, doi: 10.1038/s41586-023-05797-z.
- [17] J. Jiang, L. Xu, C. Qiu, and L.-M. Peng, "Ballistic two-dimensional InSe transistors," *Nature*, vol. 616, no. 7957, pp. 470–475, Apr 2023, doi: 10.1038/s41586-023-05819-w.
- [18] S. Song, S. Jeon, M. Rahaman, J. Lynch, D. Rhee, P. Kumar, S. Chakravarthi, G. Kim, X. Du, E. W. Blanton, K. Kisslinger, M. Snure, N. R. Glavin, E. A. Stach, R. H. Olsson, and D. Jariwala, "Wafer-scale growth of two-dimensional, phase-pure InSe," *Matter*, vol. 6, no. 10, pp. 3483–3498, 2023, doi: 10.1016/j.matt.2023.07.012.
- [19] A. AlMutairi and Y. Yoon, "Device performance assessment of monolayer  $\text{hfe}_2$ : A new layered material compatible with high- $\kappa$   $\text{hfo}_2$ ," *IEEE Electron Device Letters*, vol. 39, no. 11, pp. 1772–1775, 2018, doi: 10.1109/LED.2018.2867957.
- [20] Y. Yoon, K. Ganapathi, and S. Salahuddin, "How good can monolayer  $\text{mos}_2$  transistors be?" *Nano letters*, vol. 11, no. 9, pp. 3768–3773, 2011.
- [21] K. Nandan, A. Agarwal, S. Bhowmick, and Y. S. Chauhan, "Performance investigation of p-fets based on highly air-stable monolayer pentagonal  $\text{pdse}_2$ ," *IEEE Transactions on Electron Devices*, vol. 68, no. 12, pp. 6551–6557, 2021, doi: 10.1109/TED.2021.3119552.
- [22] G. Kresse and J. Furthmüller, "Efficient iterative schemes for ab initio total-energy calculations using a plane-wave basis set," *Phys. Rev. B*, vol. 54, pp. 11 169–11 186, Oct 1996, doi: 10.1103/PhysRevB.54.11169.
- [23] A. A. Mostofi, J. R. Yates, G. Pizzi, Y.-S. Lee, I. Souza, D. Vanderbilt, and N. Marzari, "An updated version of wannier90: A tool for obtaining maximally-localised wannier functions," *Computer Physics Communications*, vol. 185, no. 8, pp. 2309–2310, 2014, doi: 10.1016/j.cpc.2014.05.003.
- [24] S. Datta, *Quantum transport: atom to transistor*. Cambridge university press, 2005.
- [25] S. Bruzzone, G. Iannaccone, N. Marzari, and G. Fiori, "An open-source multiscale framework for the simulation of nanoscale devices," *IEEE Transactions on Electron Devices*, vol. 61, no. 1, pp. 48–53, 2014, doi: 10.1109/TED.2013.2291909.
- [26] M. Büttiker, Y. Imry, R. Landauer, and S. Pinhas, "Generalized many-channel conductance formula with application to small rings," *Phys. Rev. B*, vol. 31, pp. 6207–6215, May 1985, doi: 10.1103/PhysRevB.31.6207.
- [27] P.-C. Shen, C. Su, Y. Lin, A.-S. Chou, C.-C. Cheng, J.-H. Park, M.-H. Chiu, A.-Y. Lu, H.-L. Tang, M. M. Tavakoli *et al.*, "Ultralow contact resistance between semimetal and monolayer semiconductors," *Nature*, vol. 593, no. 7858, pp. 211–217, 2021.
- [28] W. Li, X. Gong, Z. Yu, L. Ma, W. Sun, S. Gao, Ç. Köroğlu, W. Wang, L. Liu, T. Li *et al.*, "Approaching the quantum limit in two-dimensional semiconductor contacts," *Nature*, vol. 613, no. 7943, pp. 274–279, 2023.
- [29] T. Wu and J. Guo, "Multiscale modeling of semimetal contact to two-dimensional transition metal dichalcogenide semiconductor," *Applied Physics Letters*, vol. 121, no. 2, 2022.
- [30] Y. Y. Illarionov *et al.*, "Insulators for 2D nanoelectronics: the gap to bridge," *Nature Communications*, vol. 11, no. 1, p. 3385, 2020.

- [31] Y. Y. Illarionov, A. G. Banshchikov, D. K. Polyushkin, S. Wachter, T. Knobloch, M. Thesberg, M. I. Vexler, M. Waitl, M. Lanza, N. S. Sokolov *et al.*, "Reliability of scalable mos2 fets with 2 nm crystalline caf2 insulators," *2D Materials*, vol. 6, no. 4, p. 045004, 2019.
- [32] Y. Y. Illarionov, A. G. Banshchikov, D. K. Polyushkin, S. Wachter, T. Knobloch, M. Thesberg, L. Mennel, M. Paur, M. Stöger-Pollach, A. Steiger-Thirsfeld *et al.*, "Ultrathin calcium fluoride insulators for two-dimensional field-effect transistors," *Nature Electronics*, vol. 2, no. 6, pp. 230–235, 2019.
- [33] W. Zhao *et al.*, "Field-based capacitance modeling for sub-65-nm on-chip interconnect," *IEEE Transactions on Electron Devices*, vol. 56, no. 9, pp. 1862–1872, 2009, doi: 10.1109/TED.2009.2026162.
- [34] N. Ma and D. Jena, "Carrier statistics and quantum capacitance effects on mobility extraction in two-dimensional crystal semiconductor field-effect transistors," *2D Materials*, vol. 2, no. 1, p. 015003, 2015.
- [35] A. Rahman, J. Guo, S. Datta, and M. Lundstrom, "Theory of ballistic nanotransistors," *IEEE Transactions on Electron Devices*, vol. 50, no. 9, pp. 1853–1864, 2003, doi: 10.1109/TED.2003.815366.
- [36] F. Wu, H. Tian, Z. Yan, Y. Shen, J. Ren, Y. Yang, and T.-L. Ren, "Transistor subthreshold swing lowered by 2-d heterostructures," *IEEE Transactions on Electron Devices*, vol. 68, no. 1, pp. 411–414, 2021, doi: 10.1109/TED.2020.3040350.
- [37] M. Perucchini, E. G. Marin, D. Marian, G. Iannaccone, and G. Fiori, "Physical insights into the operation of a 1-nm gate length transistor based on mos2 with metallic carbon nanotube gate," *Applied Physics Letters*, vol. 113, no. 18, p. 183507, 2018, doi: 10.1063/1.5054281.
- [38] I. M. Datye, A. Daus, R. W. Grady, K. Brenner, S. Vaziri, and E. Pop, "Strain-enhanced mobility of monolayer mos2," *Nano Letters*, vol. 22, no. 20, pp. 8052–8059, 2022, doi: 10.1021/acs.nanolett.2c01707.
- [39] C. Song, F. Fan, N. Xuan, S. Huang, G. Zhang, C. Wang, Z. Sun, H. Wu, and H. Yan, "Largely tunable band structures of few-layer InSe by uniaxial strain," *ACS Applied Materials & Interfaces*, vol. 10, no. 4, pp. 3994–4000, 2018, doi: 10.1021/acsami.7b17247.
- [40] A. K. Saha, M. Si, P. D. Ye, and S. K. Gupta, "Polarization switching in Hf<sub>0.5</sub>Zr<sub>0.5</sub>O<sub>2</sub>-dielectric stack: The role of dielectric layer thickness," *Applied Physics Letters*, vol. 119, no. 12, p. 122903, 09 2021, doi: 10.1063/5.0056448.
- [41] S. S. Cheema and Others, "Ultrathin ferroic hfo2–zro2 superlattice gate stack for advanced transistors," *Nature*, vol. 604, no. 7904, pp. 65–71, Apr 2022, doi: 10.1038/s41586-022-04425-6.
- [42] T. Agarwal, I. Radu, P. Raghavan, G. Fiori, A. Thean, M. Heyns, and W. Dehaene, "Effect of material parameters on two-dimensional materials based tfets: An energy-delay perspective," in *ESSCIRC Conference 2016: 42nd European Solid-State Circuits Conference*, 2016, doi: 10.1109/ESSCIRC.2016.7598241. pp. 55–58.
- [43] A. Naseer, K. Nandan, A. Agarwal, S. Bhowmick, and Y. S. Chauhan, "Di-metal chalcogenides: A new family of promising 2-d semiconductors for high-performance transistors," *IEEE Transactions on Electron Devices*, vol. 70, no. 5, pp. 2445–2452, 2023, doi: 10.1109/TED.2023.3261831.
- [44] K. Thakar, B. Rajendran, and S. Lodha, "Ultra-low power neuromorphic obstacle detection using a two-dimensional materials-based subthreshold transistor," *npj 2D Materials and Applications*, vol. 7, no. 1, p. 68, Sep 2023, doi: 10.1038/s41699-023-00422-z.